(Received 14 February 2025, Accepted 6 May 2025, Scheduled 10 May 2025)

Design and Analysis of a Triple-Band Stacked T-Polyimide Antenna for WBAN Applications

Kodali Rani Rudrama, Vallabhuni Tulasi Naga Kalyan*, Bachalakuri Shini, and Marampudi Vamsi

Department of Electronics and Communication Engineering, Lakireddy Bali Reddy College of Engineering Mylavaram, Andhra Pradesh, India

ABSTRACT: A low-profile, flexible and wearable microstrip patch antenna is presented for Wireless Body Area Networks (WBANs) applications. Wearability is one of the latest developments in electronic devices leading to real-time monitoring of human vital signs like blood pressure, body temperature, and pulse rates using WBAN technology. A monopole antenna with a planar rectangular and six stacked T-shaped elements is positioned on the top side of the radiating patch. A partial ground structure is incorporated at the bottom of the patch to generate triple band characteristics. The antenna is maintained with compact dimensions which are $65 \times 65 \times 0.1\,\text{mm}^3$. The antenna operates at tri-band frequencies, such as 2.7 GHz, 2.5 GHz, and 3.5 GHz, to support 5G applications. At 2.45 GHz, the directivity is 1.56 dBi; the VSWR is 1.13; the gain is 15.38; and the reflection coefficient (S_{11}) of -26.91 dB. The specific absorption rate (SAR) value of 0.160 W/kg satisfies IEEE safety requirements for biomedical applications and is much below the allowed maximum of 1.6 W/kg for 1 gram of tissue. This guarantees safe and effective operation in wearable and medical applications. The antenna has a thickness of 0.1 mm, a relative permittivity of 3.5 and provides flexibility and durability. The presentation includes the comparative analysis and the step-by-step design of the triple-band flexible antenna. Testing on a three-layer human phantom model made up of skin (2 mm), fat (8 mm), and muscle (23 mm) demonstrated the antenna's performance in terms of gain, radiation patterns, VSWR, reflection coefficient (S_{11}), and SAR. The parametric analysis, performance evaluation, simulation results, and iterative process of the antenna design are all presented in detail. Along with conclusions, comparisons to other designs, and useful estimations, the results and finalized antenna are presented. The accurate difference between measured and simulated performances indicates the antenna's reliability and efficiency, and its compact size increases flexibility in wide range of environments. The antenna was simulated using HFSS software, fabricated, and validated in an anechoic chamber and using a network analyzer.

1. INTRODUCTION

A Wireless Body Area Network (WBAN) is a network of wearable devices that wirelessly monitor and transmit health-related data. Establishing reliable and efficient remote monitoring environments is made more difficult by the usage of wireless technologies for health monitoring. The use of antennas for monitoring purposes with compact and easily integrated structures has received a lot of attention in recent years due to the increased demand for multifunctionality and multi-frequency demands. This paper presents a compact, wearable, dual-band antenna that operates at 2.4 GHz and 5.8 GHz for WBAN applications. Its semi-flexible Rogers Duroid RO3003 substrate allows for slot and partial ground adjustments to improve bandwidth and gain. Because of its high efficiency (91.4%–92.3%), steady performance under bending, and accordance to SAR safety regulations, the antenna is suitable for wearable biomedical and communication applications [1]. A dual-band flexible antenna with a self-grounding semi-circular gap is designed on a $44 \times 40 \times 0.2$ mm polyimide substrate ($\varepsilon_r = 3.5$). It covers ISM, 4G, 5G, Bluetooth, and WLAN applications and operates between 2.38 and 2.81 GHz and 4.28 and 5.10 GHz. The structure improves efficiency, gain, and bandwidth, which makes it appropriate for wearable electronic devices in military, medical, and sports applications [2]. A wearable, high-efficiency antenna is made for wireless body area networks that use a bandwidth of 320 MHz and operate at 2.40 GHz. With the use of slot architectures and a semi-flexible RO5880 substrate, it achieves 94% efficiency and 3.67 dBi gain, maintaining performance during bending and reducing SAR for wearable biomedical applications [3]. A coplanar waveguide (CPW)-fed, ultra-miniaturized ultra-wideband (UWB) wearable patch antenna that covers WiMAX, WLAN, ISM, and X-band applications operates between 3.15 and 10.55 GHz. L-shaped stubs and a shorter ground plane are included into the 98.2% compact design to improve impedance bandwidth. For e-health monitoring, its 4.2 dBi peak gain and strong performance under bending, SAR evaluation, and circuit integration make it optimal [4]. For long range (LoRa) applications, a dual-band wearable textile eighth-mode substrate integrated waveguide (SIW) antenna covering 863–870 MHz (Europe) and 902–928 MHz (North America) has been developed. Utilizing SIW cavity symmetry, the compacted construction guarantees resilience against body closeness, low cost, and compactness. Strong agreement with simulations and good isolation are confirmed by fabricated prototypes [5]. Wearable waveguide surfaces are used in this

* Corresponding author: Vallabhuni Tulasi Naga Kalyan (tulasinagakalyan@gmail.com).

small dual-branch resonator end-launcher for low-loss WBAN communications. It operates at 2.4 GHz, achieves a 0.3 dB/cm insertion loss on the human body, and fits into textiles with a 25 mm $\times$ 25 mm safety zone for electronic components. For smart clothing applications, the design makes wireless communication effective, self-sufficient, and battery-operated [6]. In order to reduce back lobes, a high front to back ratio (FBR) microstrip patch antenna with a small ground plane utilizes a resistor-loaded ground slot (RLGS) and coupled branch (CB) approaches. The concept reduces SAR while preserving excellent radiation efficiency for wearable applications, with an FBR over 38 dB. The antenna maintains its durability in the face of human body contact, ensuring stable operation [7]. Bio-inspired antenna designs, which offer improvements in bandwidth, miniaturization, and radiation patterns, are modeled after natural structures such as fractals, plant leaves, and bird feathers. These concepts, which cover frequencies from microwave to terahertz, show promise for the use in biological sensing, spectroscopy, and next-generation communication systems [8]. With the development of conductive materials, specific substrates, and SAR reduction approaches, wearable antenna technology for biomedical applications is evolving. Gain increase, bandwidth optimization, and flexible design problems for body-worn antennas are presented in this work. It highlights developments in 5G, industrial, scientific, and medical (ISM), and IoT applications, highlighting their potential in the biomedical field [9]. For WBAN and biomedical monitoring, a flexible, wearable multiple-input multiple-output (MIMO) antenna array with a meta surface-inspired design operates in the sub-6 GHz ISM band between 5.0 and 6.6 GHz. It maintains performance under bending and provides $>$ 34.8 dB isolation, 10 dBi gain, and 83% efficiency with an electromagnetic band gap (EBG) decoupling structure. Its tough, small design makes radio frequency (RF) integration easy for wearable applications [10]. In WBAN applications, wearable reconfigurable antennas facilitate multifunctional operations across different body areas by utilizing switching devices to enable dynamic changes in frequency, radiation, and polarization. Lightweight, small, and versatile, these antennas have been improved to support bending conditions, SAR regulation, and reconfigurable performance criteria [11]. Using cotton as a flexible substrate, the wearable antenna for telemedicine applications has a microstrip patch construction which operates between 4.17 and 4.25 GHz. Both on-body mode and off-body mode are supported for communicating with sensory devices, remote health monitoring, etc. For telemedicine mechanisms, copper ensures stable operation by acting as the conductive material for both the ground and antenna patch [12]. A low-profile Vivaldi MIMO antenna with a 36.44% fractional bandwidth works at 28 GHz and 30 GHz for wearable WBAN applications. It reaches SAR levels of 0.397 and 0.267 W/kg, diversity gain of $>$ 9.95 dB, and inter-element isolation of $<$ -20 dB. Its 16×20 mm^2 small size guarantees stability and conformability on the human body [13]. A wearable dual-polarized button antenna with pattern diversity operates at 2.45 GHz, 3.8 GHz, and 5.85 GHz for on-/off-body WBAN communication. It integrates a crossed-dipole and annular-ring radiator on flexible and semi-rigid substrates, ensuring ultra-wideband (UWB) coverage, high gain, and safe SAR levels. The design offers directional and omnidirectional radiation patterns for versatile applications [14]. In order to reduce frequency detuning during bending, this study suggests using a 1.575 GHz electro-textile global positioning system (GPS) antenna with a defective ground structure (DGS). By improving gain, bandwidth, and radiation efficiency, the DGS guarantees consistent performance. Its efficiency is confirmed by thorough analysis and bending tests [15]. For biomedical applications, a small circularly polarized antenna improves signal transmission for implanted medical equipment. It achieves a wide impedance bandwidth and an 18% smaller design by using ring characteristic loading. Strong radiation properties, biological compatibility, and efficient transmission up to 11.8 meters are demonstrated by tests conducted in digestive tissue [16]. The tiny UWB bow-tie antenna was designed for medical microwave imaging (MWI) and operates between 1 and 6 GHz. It has a balun circuit for minimal backward radiation and high radiation efficiency (over 80%). The antenna shows effectiveness for precise multifrequency imaging in medical diagnostics by successfully reconstructing tissue visuals using MWI techniques [17]. A wearable reconfigurable antenna with multi-mode switching that operates in sub-6 GHz, V-band, and D-band is shown in this study. It has a diamond monopole for high-rate transmissions, dual-loop antennas, and Vivaldi arrays for beam steering. High-directional radiation and wideband coverage are presented by the design [18]. For wearable wireless sensing applications like fitness tracking and health monitoring, wrist-worn antennas are growing in popularity. Sub-GHz frequencies provide long-range communication possibilities with the growth of technologies like Sigfox, NB-IoT, and LoRa WAN. However, the size restrictions of wrist-worn devices, which call for compact antennas, provide difficulties for antenna design at these frequencies. The limitations and potential developments in this field are discussed in this paper, along with antenna factors such as size, impedance bandwidth, and efficiency [19]. For wearable biomedical devices, this work presents a low-profile dual-port orthomode antenna that allows for in-band full-duplex communication at 6 GHz with good Tx/Rx isolation ($>$ 35 dB). Because of its excellent front-to-back ratios, stability in radiation patterns, and resistance to bending, it is suitable for wearable applications [20]. A flexible 2×2 metasurface-based rectenna array that operates at 2.45 GHz is presented in this study as a wireless power source for low-power wearable medical sensors. The rectifier demonstrates its potential for wearable medical applications with up to 56% power conversion efficiency, while the meta-patch antenna reaches 7 dB gain, 77% efficiency, and 120 MHz bandwidth [21]. Fresnel-zone focused antenna arrays have been explored with a focus on biomedical applications' safety and health [22]. A flexible, omnidirectional, dual-band wearable antenna with a low profile is proposed for Wireless Body Area Network (WBAN) applications. Built on an RT/duriod 5870 substrate, it has a small size and an enhanced impedance bandwidth, operating at 2.45 GHz and 5.2 GHz. The antenna is perfect for wearable WBAN devices because it performs well, has good gain, high efficiency, and behaves robustly under bending

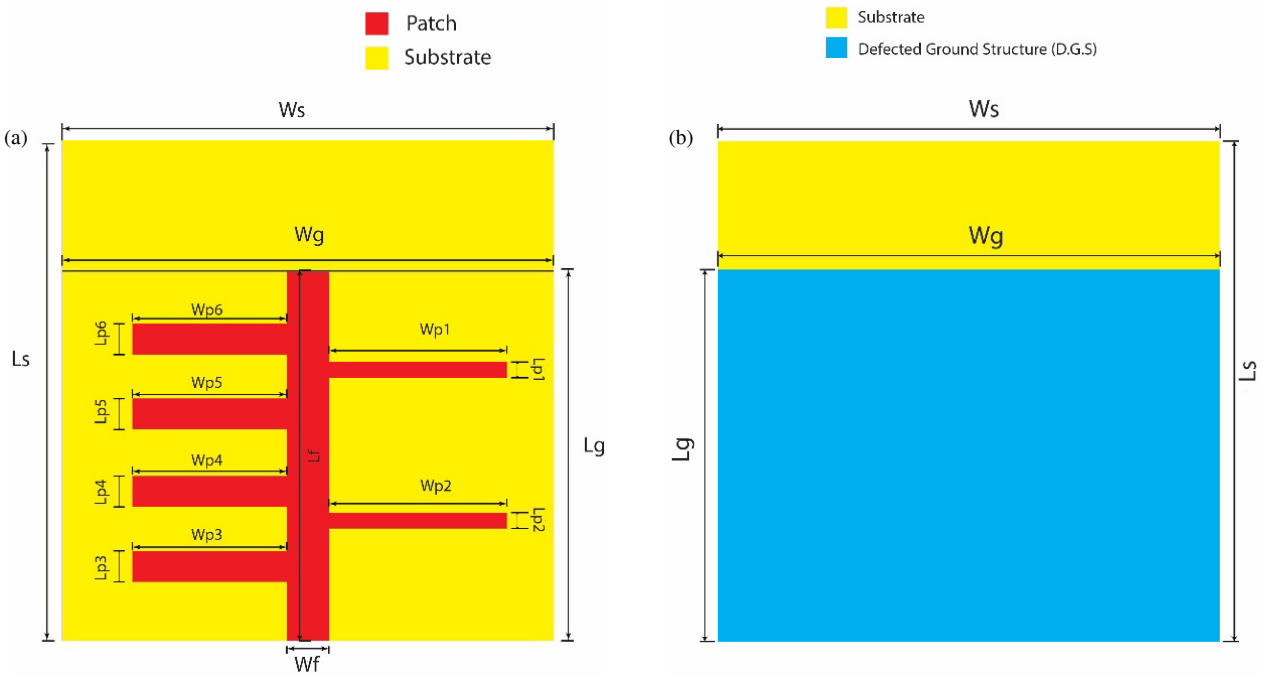

FIGURE 1. Proposed antenna. (a) Patch of the antenna. (b) Defected Ground Structure.

and body stress [23]. A stretchable and flexible wearable antenna for 5G applications operating at 3.5 GHz uses polydimethylsiloxane (PDMS) and a specially made silver alloy. An air gap PDMS substrate is incorporated into the design to increase bandwidth and gain while preserving performance up to 20% under bending and stretching. Additionally, the study evaluates the antenna's specific absorption rate (SAR) to ensure that it is safe for human use [24]. A wearable broadband textile antenna enables both near-field and far-field wireless power transfer (WPT) at the same time. It maintains compactness and substrate independence by combining a broadband monopole for ultra-high-frequency (UHF) far-field WPT and an inductive coil for high-frequency (HF) near-field WPT. The system effectively feeds a Bluetooth Low Energy node with up to 80% near-field WPT efficiency and 40% far-field rectenna efficiency [25]. A CPW-fed wearable antenna with an artificial magnetic conductor (AMC) array operates at 2.45 GHz and 5.5 GHz, achieving enhanced gain and decreased SAR, making it appropriate for WLAN and WBAN applications [26]. By using bone attenuation analysis, it presents a textile-based UWB wearable monopole antenna with a neural network that operates at 4.9–12.6 GHz and achieves 87% accuracy in osteoporosis detection [27].

This paper is structured in the following manner. The antenna design is thoroughly explained in Section 2, which also includes parametric analysis, performance evaluation, and simulation results for reflection coefficient (S_{11}), voltage standing wave ratio (VSWR), gain, directivity, SAR evaluation, and radiation pattern analysis. An additional discussion of the iterative procedure used to arrive at the final antenna design is provided. Results and discussions of the finished antenna are presented in Section 3. Finally, Section 4 presents a summary of the main conclusions, compares the suggested antenna with other substrates and existing designs, and provides practical predictions from the study.

2. ANTENNA DESIGN

2.1. Antenna Model

The proposed triple-band polyimide-based flexible antenna is illustrated in Figure 1. To enhance the antenna's bandwidth, a defected ground structure (DGS) is applied to three-fourths of the bottom ground plane. Additionally, six patch stubs are placed symmetrically on two sides of the top patch: four on the left and two on the right, each measuring 4 mm in length. A 50 Ω coaxial feed supplies power to the antenna. The substrate is a 0.1 mm thick with polyimide-based material that offers the required flexibility. The antenna's radiating element is excited by a DGS. Standard equations for microstrip patch antennas were used to determine the length and width of the patch dimensions.

For example, the patch width equation is shown in Equation (1),

$$w = \frac{c}{2f_0\sqrt{\frac{\epsilon_r+1}{2}}} \tag{1}$$

The patch length equation is shown in Equation (2),

$$L = \frac{c}{2f_0\sqrt{\epsilon_r}} \tag{2}$$

where ϵ_{eff} represents the effective dielectric constant, which is shown in Equation (3),

$$\epsilon_{eff} = \frac{\epsilon_\gamma+1}{2} + \frac{\epsilon_r-1}{2}\left[\sqrt{1+12\left(\frac{h}{w}\right)}\right] \tag{3}$$

TABLE 1. Proposed antenna's design parameters in Figure 1(a) and 1(b).

Dimensions (unit: mm)				
$W_G = 65$	$W_F = 5.225$	$L_{p2} = 2$	$L_{p4} = 4$	$L_{p6} = 4$
$L_G = 48.75$	$L_F = 35$	$W_{p2} = 23.6125$	$W_{p4} = 20.6375$	$W_{p6} = 20.6375$
$W_S = 65$	$L_{P1} = 2$	$L_{p3} = 4$	$L_{p5} = 4$	$f_O = 2.45$
$L_S = 65$	$W_{P1} = 23.6125$	$W_{p3} = 20.6375$	$W_{p5} = 20.6375$	$h = 0.1$

The suggested triple-band antenna was implemented using a polyimide material with a dielectric constant of $\varepsilon r = 3.5$. Overall, the antenna measures 65 mm by 65 mm by 0.1 mm. Analyses and designs were conducted using the ANSYS HFSS software 2024R2 student version. Table 1 offers an overview of the precise dimensions of the proposed antenna following detailed parametric simulations.

2.2. Antenna Performance Evaluation

A human phantom model with three layers is constructed using square boxes, as illustrated in Figure 2. The antenna is embedded between the layers of fat tissue, and the skin tissue is placed above it. The muscle tissue is then positioned below the antenna. Due to its slightly larger dimensions than the antenna, the model can be used for SAR calculations. Accurately representing the human phantom involves modeling the relative permittivity and conductivity of the skin, muscle, and fat of the human body. The thickness of muscle is 8 millimeters, fat 2 millimeters, and skin 23 millimeters. On-body antenna placement involves positioning the antenna outside the human body. The 2.45 GHz characteristics of human body tissues are listed in Table 2. There are noticeable variations in the antenna's resonance frequency because the dielectric constant of human tissues is high.

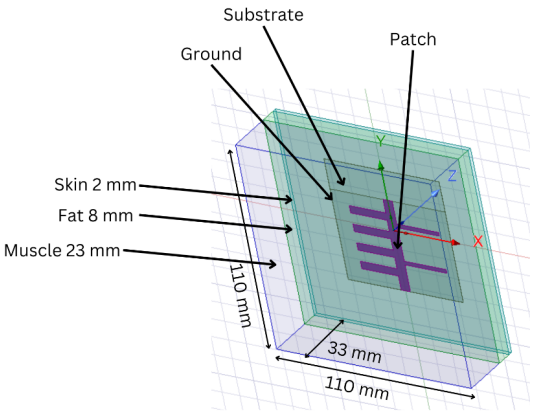

FIGURE 2. Human phantom model.

TABLE 2. Human phantom model parameters.

Human cell	Permittivity ($\in_r$)	Conductivity (S/m)
Fat	5.28	0.1
Skin	31.29	5.0138
Muscle	52.79	1.705

2.3. Parametric Analysis

To optimize the antenna's reflection coefficient (S_{11}), a detailed parametric analysis was conducted by systematically varying the dimensions of the patch geometry. The optimal dimensions obtained from the study are presented in Table 1. In the initial design (Iteration 1), the antenna featured three patch stubs with lengths of 1.25 mm, 2 mm, and 4 mm: two on the left and one on the right. This configuration resulted in a reflection coefficient (S_{11}) of -15 dB. To enhance performance, the number of patch stubs was increased to four, with three on the left and one on the right. This modification significantly reduced the reflection coefficient (S_{11}) compared to the initial design. In Iteration 3, the number of patch stubs was further increased to six, with four on the left and two on the right. All left-side patch stubs maintained uniform width and length, while the dimensions of the right-side stubs were slightly reduced to further optimize the reflection coefficient (S_{11}). To improve antenna performance, a DGS was also added. As a result of these design enhancements, the final antenna achieved a substantial improvement with a reflection coefficient (S_{11}) of -26.39 dB. Figure 3 displays the comprehensive parametric analysis. In Iteration 1, two bands were observed: Band 1 (2.25–2.35 GHz) and Band 2 (2.85–2.95 GHz). In Iteration 3, three bands were achieved: Band 1 (2.45–2.58 GHz), Band 2 (2.58–2.70 GHz), and Band 3 (3.55–3.58 GHz). Figure 4 depicts the reflection coefficient (S_{11}) results for Iteration 1 and Iteration 3.

2.4. Simulation Results

2.4.1. Reflection Coefficient (S_{11}) Evaluation

Reflection coefficient (S_{11}) measures power loss due to impedance mismatches in antenna design. The 50 Ω input impedance ensures optimal performance. Simulation results show a -26.91 dB reflection coefficient (S_{11}) at 2.45 GHz, as illustrated in Figure 5, indicating efficient power radiation.

2.4.2. VSWR Evaluation

The antenna's low VSWR of 1.13 at 2.45 GHz, indicating excellent matching conditions and minimal reflection loss, as shown in Figure 6, allows it to be utilized in WBANs and healthcare applications.

2.4.3. Gain Measurement Evaluation

Radiation efficiency is indicated by antenna gain, as shown in Figure 7. Due to tissue absorption, wearable biomedical applications may experience negative gain. The antenna's 3D gain

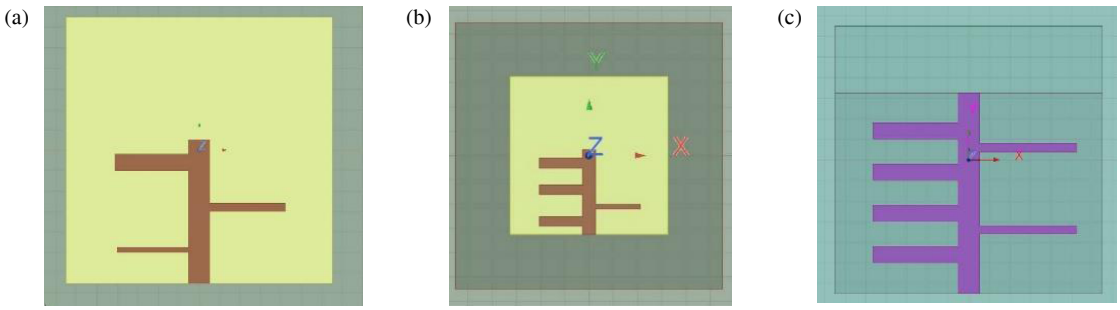

FIGURE 3. Patch geometry of the antenna across design iterations: (a) Iteration 1 without DGS. (b) Iteration 2. (c) Iteration 3 with DGS.

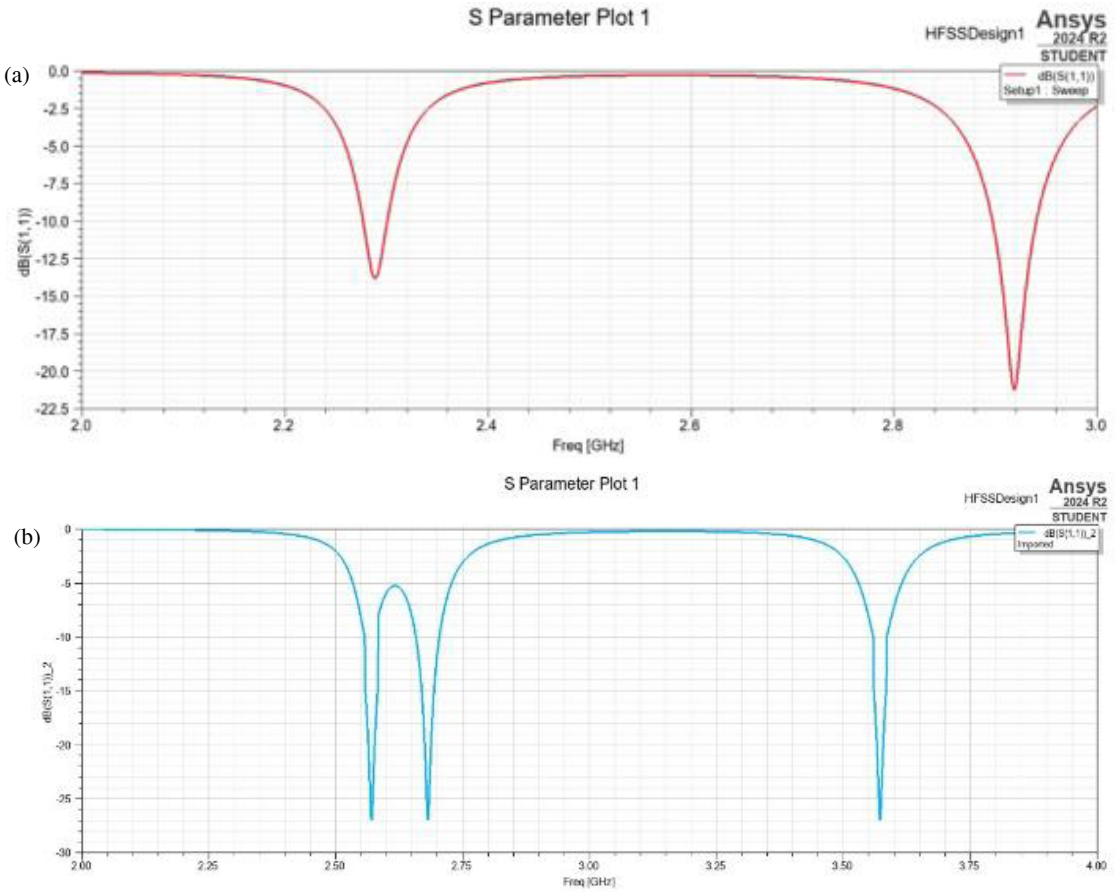

FIGURE 4. Reflection coefficient (S_{11}) graphs for Iteration 1 without DGS and Iteration 3 with DGS.

on a human phantom was 15.38 dB; however, it still performed well in radiation for WBAN applications, with an omnidirectional pattern that peaks at 0°.

2.4.4. Directivity Analysis

The antenna's directivity, which is 1.55 dBi in Figure 8, is adequate for wearable biomedical applications. It has few sidelobes and transmits signals effectively in the ISM band.

2.4.5. Evaluation of SAR

In accordance with safety regulations for biomedical applications, the 2.45 GHz designed antenna obtained a mass of one gram of tissue, the Specific Absorption Rate (SAR) was 0.168 W/kg, which is far lower than IEEE safety guidelines of 1.6 W/kg. The SAR distribution and safe antenna operation in the human phantom model is presented in Figure 9.

The formula for calculating SAR is shown in Equation (4),

$$SAR = \frac{\sigma |E|^2}{\rho} \tag{4}$$

2.4.6. Radiation Patterns Evaluation

The antenna's radiation pattern at 2.45 GHz was examined using HFSS in polar coordinates. Figure 10 illustrates how an-

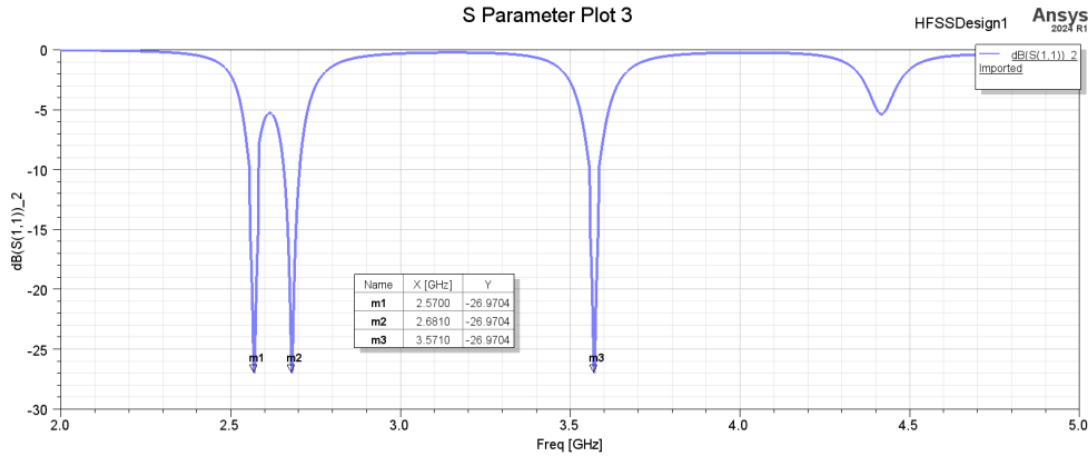

FIGURE 5. Reflection coefficient (S_{11}) plot.

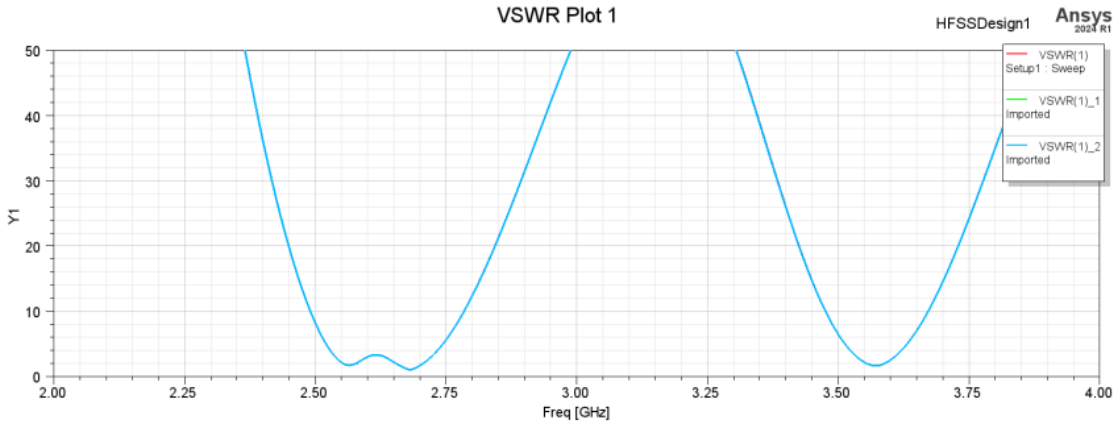

FIGURE 6. VSWR plot.

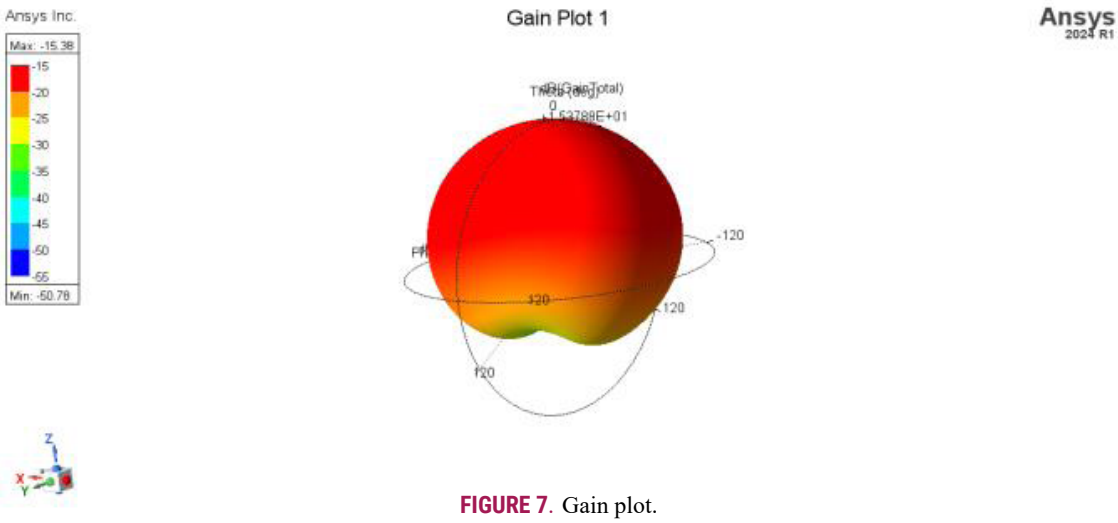

FIGURE 7. Gain plot.

tenna orientation affects performance by evaluating phase angles at 0° and 90° to analyze the radiation characteristics. Higher directivity with sidelobes was seen in the red curve (phi = 90°), whereas greater coverage and lower directivity were shown in the green curve (phi = 0°).

3. RESULTS AND DISCUSSION

The polyimide-based proposed triple-band flexible antenna has been developed and verified properly in accordance with the measurements given in Table 1. Figure 11(a) shows the constructed antenna prototype, while Figure 11(b) illustrates the

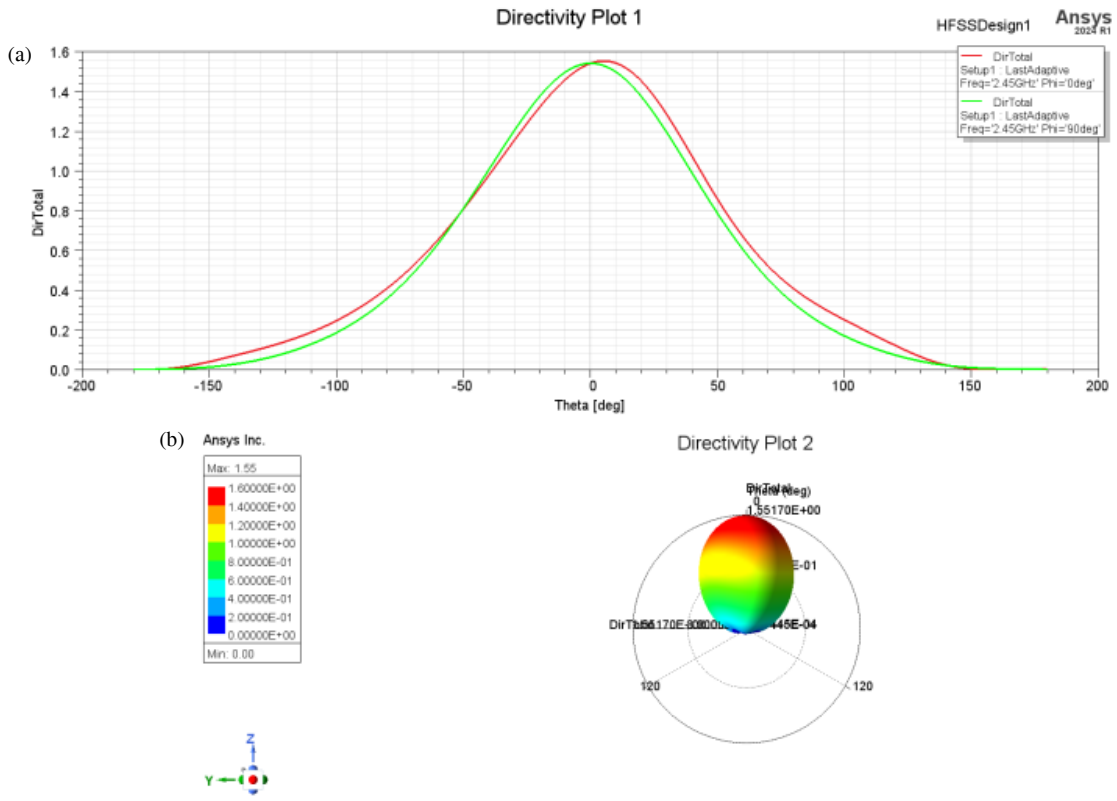

FIGURE 8. Directivity plots of the antenna at 2.45 GHz: (a) 2D Directivity plot, (b) 3D Directivity plot.

TABLE 3. Performance comparison of the proposed antenna using different substrates at 2.45 GHz.

Substrate	Operating Frequency (f_0)	Reflection Coefficient (S_{11})	VSWR	Gain (dBi)
Polyimide	2.45 GHz	−26.91	1.09	15.38
Teflon	3.8 GHz	−9.56	1.99	1.1
FR4_epoxy	4.2 GHz	−31.49	1.05	15.18
Rogers RT/duriod 5880 (tm)	9 GHz	−6.6	2.7	2.1

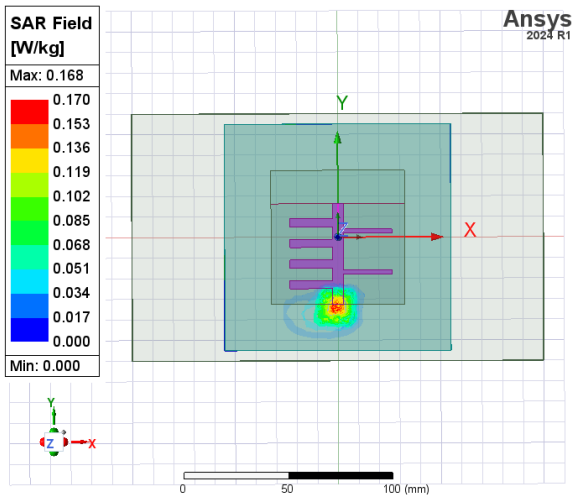

FIGURE 9. SAR distribution analysis.

S-parameters measurement configuration within an anechoic chamber. The model and Figure 12 display a comparison of measurements using the reflection coefficient S_{11} and VSWR. The results indicate that the polyimide antenna exhibits a gain of 15.38 dBi at a 2.5 GHz frequency. Similarly, Figure 13(a) compares the simulated and measured gains versus frequency curves, and Figure 13(b) compares the simulated and measured radiation pattern graphs.

This section presents a comparative analysis of the outcomes of the simulation and measurement using gain, radiation pattern, VSWR, and reflection coefficient (S_{11}). Figure 12 illustrates the S_{11} and VSWR comparisons, demonstrating good alignment between simulated and measured data, with minor deviations due to fabrication errors and connector faults. Both analyses maintained a VSWR between 1 and 2 within the intended frequency range.

The study examines the impact of skin conditions on antenna performance using HFSS tools and SAR simulations. It

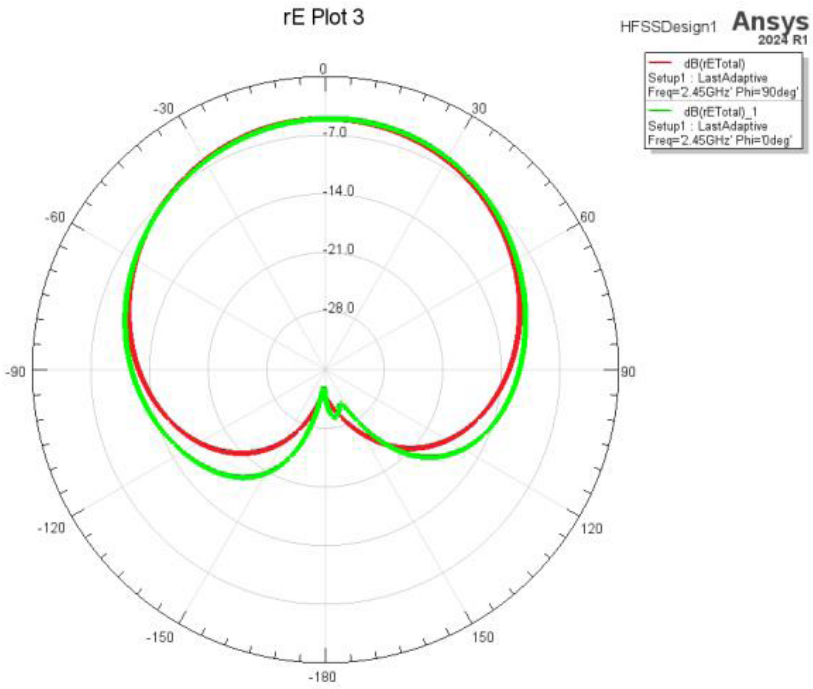

FIGURE 10. Radiation patterns plot.

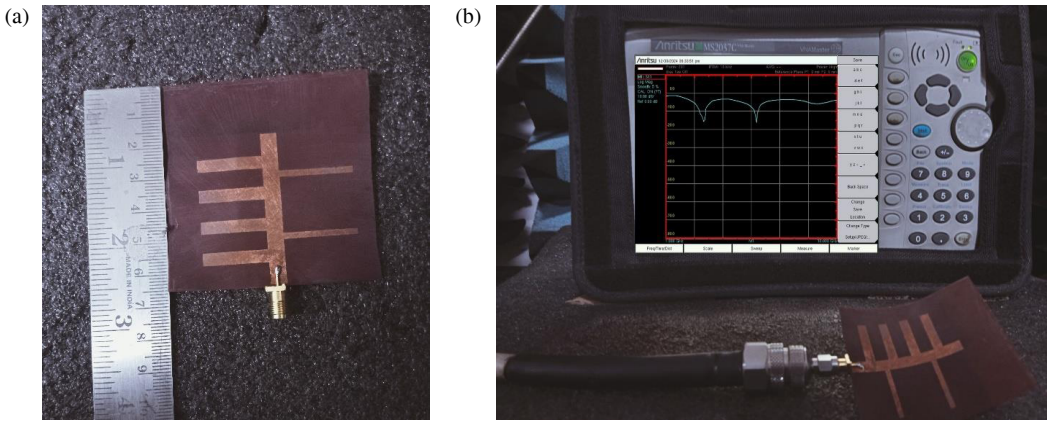

FIGURE 11. Proposed tri-band polyimide antenna: (a) Prototype; (b) S_{11} measurement setup in Anechoic chamber.

is found that off-body placement results in excellent impedance matching and minimal signal reflection, while on-body placement results in reduced VSWR and reflection coefficient (S_{11}); radiation and antenna gain efficiencies also show changes. Gain remains stable in off-body cases, but radiation efficiency declines from 94.32% off-body to 82.57% on-body due to the energy absorption by bodily tissues.

These findings highlight the influence of skin conditions and proximity to the human body on the antenna's overall performance. The evaluation of the proposed antenna using different substrates is presented in Table 3, where all values of reflection coefficient (S_{11}), VSWR, and gain were obtained at the operating frequency of 2.45 GHz to ensure a fair and consistent comparison. This table also illustrates how the inclusion of patch stubs significantly reduces the antenna size while maintaining effective operational bandwidth. Substrates such as Teflon, FR4 epoxy, Polyimide, and Rogers RT/Duroid 5880 were included in the analysis.

Among them, the polyimide-based antenna demonstrates superior performance, achieving a VSWR of 1.03 and a reflection coefficient (S_{11}) of -26.94 dB at 2.45 GHz, all within a compact footprint of $65 \times 65\,\text{mm}^2$. These results underscore its effectiveness in maintaining optimal performance while minimizing antenna dimensions. Table 4 provides a detailed performance comparison between the proposed antenna and other existing designs from prior studies [6, 12, 14], highlighting the compactness and superior VSWR of our proposed structure.

3.1. Evaluation of the Fabricated Antenna on the Body

The constructed antenna was positioned on a human body model to assess its performance in on-body scenarios. As illus-

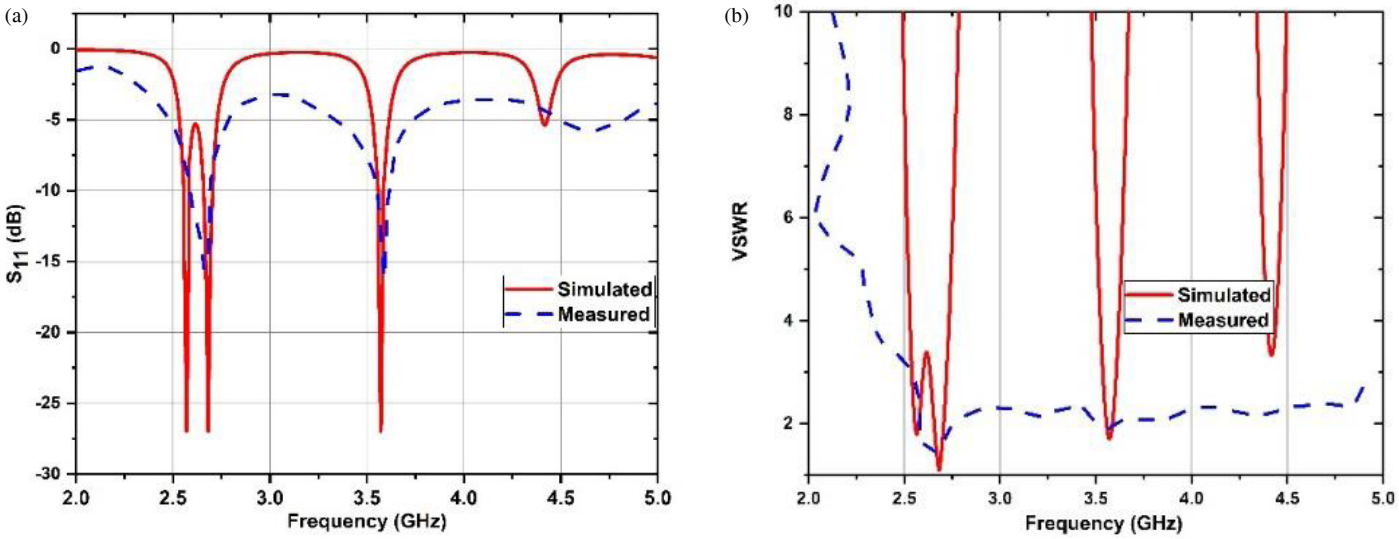

FIGURE 12. Simulation and measurement comparison: (a) S_{11} vs frequency; (b) VSWR.

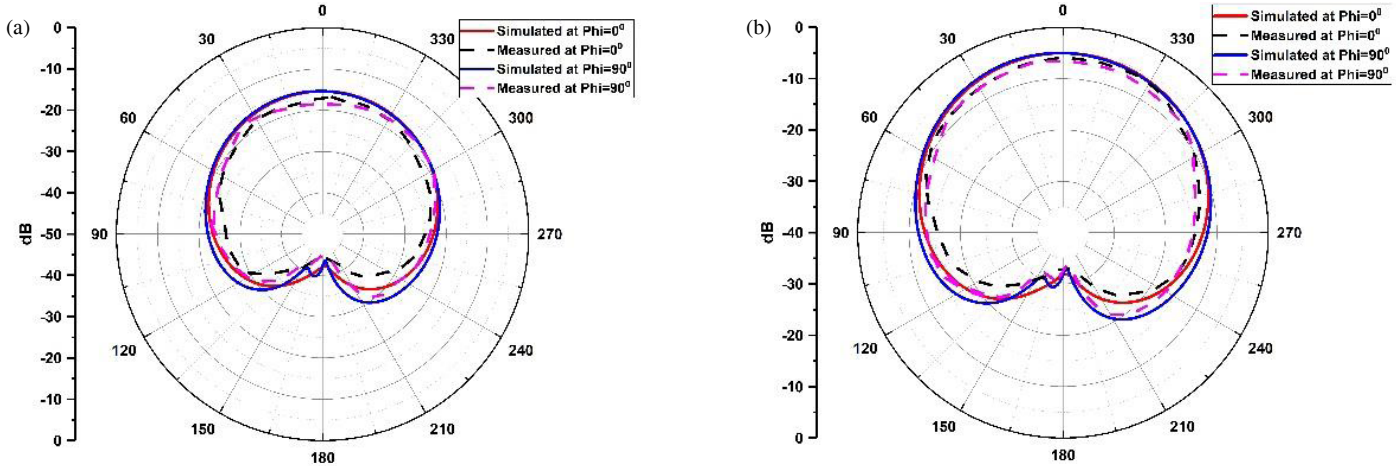

FIGURE 13. Simulation and measurement comparison: (a) Gain vs frequency; (b) Radiation pattern.

TABLE 4. Performance comparison of proposed and existing antennas.

Reference	Operating Frequency (GHz)	Size in (mm)	Reflection Coefficient (S_{11}) (dB)	VSWR
This study	2.45	65×65	-26.91	1.03
[12]	4.25	90×100	-22.13	1.1
[6]	2.45	25×25	-10.52	1.8
[14]	2.45	40×40	-21.52	1.1

trated in Figure 14, the return loss was assessed and contrasted with that of the independent (free-space) arrangement. In the on-body situation, only one resonance peak is apparent because of the graph's scaling modification; nonetheless, the return loss stays mostly stable, with a minor variation. At 2.45 GHz, the return loss on the body is recorded at -20.87 dB, while in the stand-alone scenario, it is -26.94 dB. This shows a significant drop in performance, anticipated because of the effect of human tissue. These results are quantitatively presented in Table 5, which compares return loss, VSWR, directivity, and radiation efficiency between free-space and on-body conditions. The fluctuation shows the usual electromagnetic absorption by body layers that slightly modifies the antenna's impedance matching. An overview of the main performance metrics in both scenarios is provided below.

These findings verify that although the antenna shows minor performance decline when being placed on the body — because of tissue interaction — it still functions well and is appropriate for wearable WBAN uses.

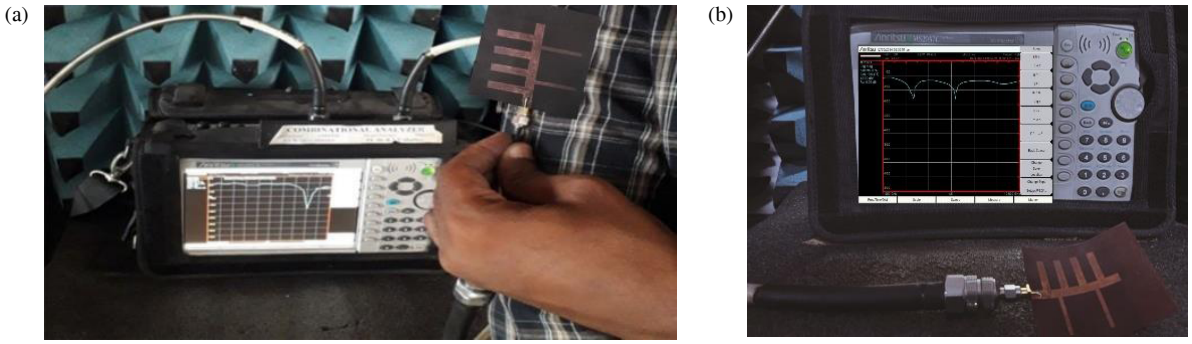

FIGURE 14. Measurement of return loss in (a) on body antenna and (b) off body antenna.

TABLE 5. Comparison of return loss and other parameters for on-body and off-body antenna configurations.

Parameter	Free Space (Independent)	On-Body
Reflection Coefficient (S_{11})	−26.94 dB	−20.87 dB
VSWR	1.09	1.23
Directivity	15.38 dBi	14.23 dBi
Radiation Efficiency	94.95%	81.94%

4. CONCLUSION

This paper presents a compact wearable antenna with low reflection coefficient (S_{11}), good VSWR, and minimal SAR within safety limits, which operates at 2.45 GHz for wireless and biomedical applications. The design maintains a minimal dimension of 65×65 mm^2 while exhibiting respectable performance in gain, directivity, and radiation patterns. The safety of the antenna for use in biomedical applications is confirmed by tests using human body phantoms. With a 50 Ω impedance, the inset feed approach facilitates feeding and ensures flat structures. In line with developments in digital healthcare and new technologies like 5G, future research will focus on increasing bandwidth and efficiency.

REFERENCES

[1] Musa, U., S. M. Shah, H. A. Majid, I. A. Mahadi, M. K. A. Rahim, M. S. Yahya, and Z. Z. Abidin, "Design and analysis of a compact dual-band wearable antenna for WBAN applications," *IEEE Access*, Vol. 11, 30 996–31 009, 2023.

[2] Yu, Z., R. Niu, G. Zhang, R. Sun, Z. Lin, Y. Li, and X. Ran, "A wearable self-grounding slit antenna for ISM/4G/5G/bluetooth/WLAN applications," *IEEE Access*, Vol. 11, 87 930–87 937, 2023.

[3] Waly, M. I., A. Smida, N. A. Aljarallah, R. Ghayoula, A. S. Negm, S. Muhammad, J. J. Tiang, and A. Iqbal, "Advancement of a high-efficiency wearable antenna enabling wireless body area networks," *IEEE Access*, Vol. 11, 138 325–138 335, 2023.

[4] Modak, S., V. Kaim, T. Khan, B. K. Kanaujia, L. Matekovits, and K. Rambabu, "Design and performance measurement of worn-on-body instrumental ultra-miniaturized uwb wearable patch for e-health monitoring," *IEEE Access*, Vol. 12, 25 719–25 730, 2024.

[5] Casula, G. A., G. Montisci, and G. Muntoni, "A novel design for dual-band wearable textile eighth-mode SIW antennas," *IEEE Access*, Vol. 11, 11 555–11 569, 2023.

[6] El Bacha, M., F. Ferrero, and L. Lizzi, "Design of a dual-branch resonator end-launcher for low-loss WBAN communications using wearable waveguide surfaces," *IEEE Open Journal of Antennas and Propagation*, Vol. 5, No. 1, 67–72, Feb. 2024.

[7] Yu, S.-W., X. Zhang, Q.-S. Wu, L. Zhu, T. Yuan, and Q.-H. Jiang, "Low-SAR and high-FBR patch antenna with small ground size for wearable devices," *IEEE Open Journal of Antennas and Propagation*, Vol. 5, No. 1, 124–129, Feb. 2024.

[8] Azam, F., S. I. H. Shah, S. Bashir, and S. Koziel, "Review of recent advancement on nature/bio-inspired antenna designs," *IEEE Access*, Vol. 12, 37 493–37 512, 2024.

[9] Giftsy, A. L. S., U. K. Kommuri, and R. P. Dwivedi, "Flexible and wearable antenna for biomedical application: Progress and opportunity," *IEEE Access*, Vol. 12, 90 016–90 040, 2023.

[10] Althuwayb, A. A., M. Alibakhshikenari, B. S. Virdee, N. Rashid, K. Kaaniche, A. B. Atitallah, A. Armghan, O. I. Elhamrawy, C. H. See, and F. Falcone, "Metasurface-inspired flexible wearable MIMO antenna array for wireless body area network applications and biomedical telemetry devices," *IEEE Access*, Vol. 11, 1039–1056, 2022.

[11] Musa, U., S. M. Shah, H. A. Majid, Z. Z. Abidin, M. S. Yahya, S. Babani, and Z. Yunusa, "Recent advancement of wearable reconfigurable antenna technologies: A review," *IEEE Access*, Vol. 10, 121 831–121 863, 2022.

[12] Jayasudha, F. V., I. R. Sheeba, K. Srilatha, I. M. S. Sanju, and P. Chitra, "Designing an wearable antenna for telemedicine applications," in *2024 10th International Conference on Communication and Signal Processing (ICCSP)*, 1291–1296, Melmaruvathur, India, Apr. 2024.

[13] Ahmad, J., M. Hashmi, A. Bakytbekov, and F. Falcone, "Design and analysis of a low profile millimeter-wave band vivaldi MIMO antenna for wearable WBAN applications," *IEEE Access*, Vol. 12, 70 420–70 433, 2024.

[14] Le, T. T., Y.-D. Kim, and T.-Y. Yun, "Wearable pattern-diversity dual-polarized button antenna for versatile on-/off-body communications," *IEEE Access*, Vol. 10, 98 700–98 711, 2022.

[15] Zaidi, N. I., N. H. A. Rahman, M. F. Yahya, M. S. A. Nordin, S. Subahir, Y. Yamada, and A. Majumdar, "Analysis on bending performance of the electro-textile antennas with bandwidth enhancement for wearable tracking application," *IEEE Access*, Vol. 10, 31 800–31 820, 2022.

[16] Ou, R.-X. and W.-L. Yu, "Design of small circular polarized antenna with ring descriptive loading for biomedical applications,"

IEEE Access, Vol. 11, 130 840–130 849, 2023.

[17] Fiser, O., V. Hruby, J. Vrba, T. Drizdal, J. Tesarik, J. Vrba Jr, and D. Vrba, "UWB bowtie antenna for medical microwave imaging applications," *IEEE Transactions on Antennas and Propagation*, Vol. 70, No. 7, 5357–5372, Jul. 2022.

[18] Chung, M.-A., C.-W. Lin, C.-W. Yang, and I.-P. Meiy, "Wearable reconfigurable antennas with multi-mode switching for Sub-6 GHz, V-band, and D-band applications," *IEEE Access*, Vol. 12, 115 448–115 464, 2024.

[19] Kumar, S., G. Moloudian, R. B. V. B. Simorangkir, D. R. Gawade, B. O'Flynn, and J. L. Buckley, "Sub-GHz wrist-worn antennas for wireless sensing applications: A review," *IEEE Open Journal of Antennas and Propagation*, Vol. 5, No. 5, 1258–1281, Oct. 2024.

[20] Wu, Y., G. Mackertich-Sengerdy, S. Soltani, S. D. Campbell, D. Yang, and D. H. Werner, "Low profile orthomode full-duplex antenna for wearable biomedical communication," *IEEE Access*, Vol. 12, 40 092–40 104, 2024.

[21] Alkhalaf, H. Y., M. Y. Ahmad, H. Ramiah, A. K. M. Z. Hossain, S. M. K. Azam, and A. Thiha, "Flexible meta-patch rectenna array for energizing low-power wearable medical sensors," *IEEE Access*, Vol. 12, 121 570–121 585, 2024.

[22] Buonanno, G. and S. Costanzo, "Fresnel-zone focused antenna arrays: Tolerance analysis for biomedical applications," *IEEE Transactions on Antennas and Propagation*, Vol. 71, No. 9, 7261–7272, Sep. 2023.

[23] Khan, M. A., W. T. Sethi, W. A. Malik, A. Jabbar, M. A. Khalid, A. M. Almuhlafi, and M. Himdi, "A comprehensive analysis of low-profile dual band flexible omnidirectional wearable antenna for WBAN applications," *IEEE Access*, Vol. 12, 45 187–45 201, 2024.

[24] Salleh, S. M., M. F. Ain, Z. Ahmad, I. S. Z. Abidin, L. Y. Seng, and M. N. Osman, "Stretchable and bendable polydimethylsiloxane-silver composite antenna on pdms/air gap substrate for 5g wearable applications," *IEEE Access*, Vol. 11, 133 623–133 639, 2023.

[25] Wagih, M., A. Komolafe, A. S. Weddell, and S. Beeby, "Broadband compact substrate-independent textile wearable antenna for simultaneous near-and far-field wireless power transmission," *IEEE Open Journal of Antennas and Propagation*, Vol. 3, 398–411, 2022.

[26] Reddy, R. N., N. V. K. Rao, and D. R. Krishna, "An AMC-backed dual-band gain-enhanced wearable antenna with SAR for WLAN/WBAN applications," *Progress In Electromagnetics Research C*, Vol. 146, 55–64, 2024.

[27] Ouf, E. G., A. S. A. El-Hameed, A. G. Seliem, and S. M. Elnady, "Wearable antenna system for osteoporosis detection and monitoring using machine learning," *Progress In Electromagnetics Research C*, Vol. 146, 21–32, 2024.